

Extended flat band and many-body interactions in Kekulé-ordered graphene

Changhua Bao^{1,*}, Hongyun Zhang^{1,*}, Xi Wu², Shaohua Zhou¹, Qian Li¹, Pu Yu^{1,3}, Jia Li², Wenhui Duan^{1,3} & Shuyun Zhou^{1,3,†}

¹*State Key Laboratory of Low-Dimensional Quantum Physics and Department of Physics, Tsinghua University, Beijing 100084, P. R. China*

²*Shenzhen Geim Graphene Center and Institute of Materials Research, Tsinghua Shenzhen International Graduate School, Tsinghua University, Shenzhen 518055, P. R. China*

³*Frontier Science Center for Quantum Information, Beijing 100084, P. R. China*

**These authors contributed equally to this work.*

†Corresponding author. E-mail: syzhou@mail.tsinghua.edu.cn

While graphene shows a characteristic conical dispersion with a vanishing density of states (DOS) near the Fermi energy E_F , it has been suggested that under extremely-high doping ($\sim 1/4$), the extended flat band can be shifted to near E_F , resulting in a diverging DOS with strong many-body interactions and electronic instabilities. Although such highly-doped graphene has attracted tremendous research interests, so far the experimental demonstration of doping-induced flat band as well as its associated intriguing phenomena remains rather limited. Here, we report the observation of an extended flat band around the M point in a Li-intercalated graphene, in which the Li ions not only dope graphene with a high electron concentration, but also induce a Kekulé order which breaks the chiral symmetry. At

such high electron doping, pronounced electron-phonon and electron-electron interactions are clearly identified by the notable kinks in the band dispersion and a strong reduction of the band width. Moreover, by following the evolution of the band structure upon Li intercalation, we find that the flat band and the Kekulé order, with the characteristic flat band near M and folded Dirac cones near Γ respectively, emerge simultaneously, which indicates that they are strongly coupled. Our work identifies Li-intercalated graphene as a fertile platform for investigating the unique physics of the extended flat band, strong many-body interactions as well as the Kekulé order.

In solids, flat band with a high density of states (DOS) near the Fermi energy E_F can enhance many-body interactions such as electron-phonon (el-ph) interaction and electron-electron correlation, thereby increasing instabilities toward exotic ordered states. For example, in magic-angle twisted bilayer graphene (MABLG) ¹, the flat band can be induced through hybridization of the Dirac cones via the moiré superlattice potential. The effect of electron-electron correlation becomes important, and novel phenomena such as superconductivity ², Mott insulator ³ and charge order ⁴ have been discovered. Instead of band hybridization near the Dirac point, a different strategy for inducing a flat band is to shift the van Hove singularity (VHS) at energy far above the Dirac point of graphene (see Fig. 1A for schematic band structure) to E_F by electron doping to near the 1/4 filling. The physics near 1/4 doping of graphene has attracted extensive interests, and intriguing phenomena such as instabilities toward d -wave superconductivity by repulsive electron-electron interaction ⁵⁻⁷, topological superconductivity ⁸, and chiral spin density wave ^{9,10} have been predicted.

In graphene, the π^* band VHS is at ~ 3 eV above the Dirac point ¹¹ (see schematic electronic structure in Fig. 1A), and an extremely high electron doping of $\sim 4.6 \times 10^{14}$ cm⁻² is required to shift it to E_F . Experimentally, electron doping of graphene can be achieved by adsorption of alkali metals such as K, Cs, Ca, Li ¹²⁻¹⁷ or intercalation of Gd, Yb ¹⁸⁻²¹. It has been shown recently that combining Yb intercalation with K adsorption can dope the graphene sample beyond the VHS ²¹. However, the Dirac cone of graphene is also severely distorted due to the hybridization with the 4f orbital of the intercalated Yb. Here we report the experimental observation of extended flat band below E_F in a Li-intercalated graphene by angle-resolved photoemission spectroscopy (ARPES), where the graphene Dirac cone remains intact without hybridization with the intercalated Li. Interestingly, the intercalated Li ions also induce a Kekulé order which breaks the chiral symmetry (CSB) ²², and here we focus on the extended flat band and many-body interactions. The VHS at the M point is tuned to below E_F (-20 meV), and significant band renormalization is observed as a result of strong el-ph and electron-electron interaction. Moreover, to check if there is any connection between the flat band and the Kekulé order, we monitor the evolution of the extended flat band near M and folded Dirac cone near Γ upon Li intercalation. Our results show that both the flat band and folded Dirac cones exhibit the same trend and emerge at the same doping, suggesting a strong connection between the flat band and the Kekulé order. Our work reports the coexistence and co-development of extended flat band and Kekulé order in Li-intercalated graphene, and provides opportunities for investigating their interplay.

The Kekulé-ordered graphene is obtained by intercalating Li to monolayer graphene on SiC substrate (see Methods) ²²⁻²⁴, forming Li-intercalated bilayer graphene as schematically illustrated

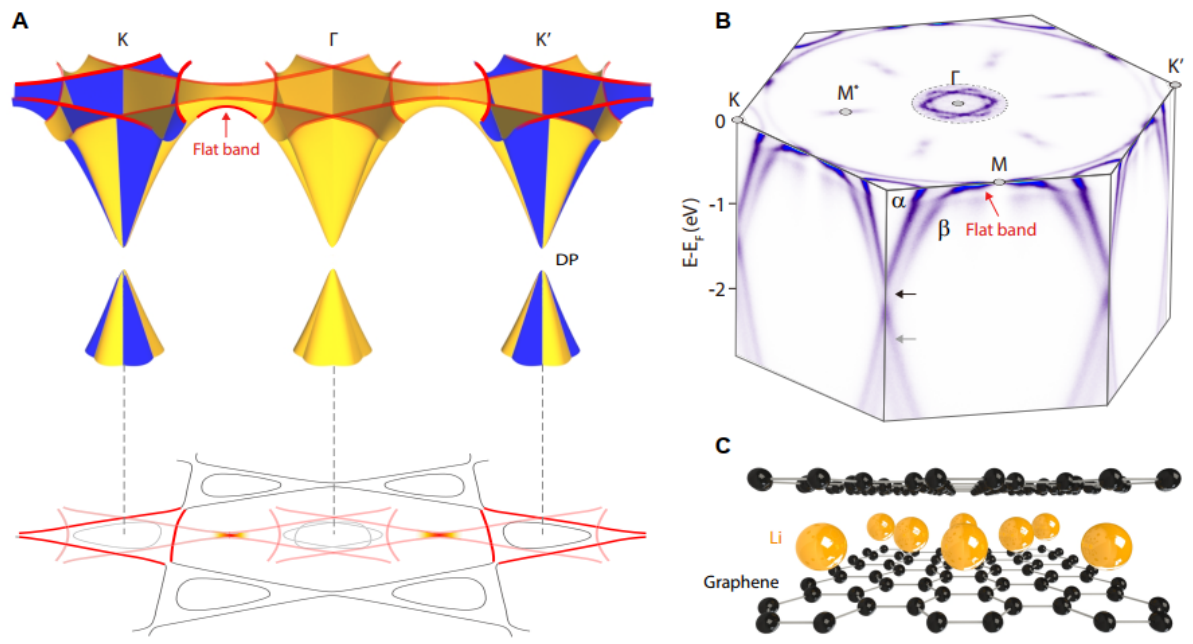


Figure 1: Extended flat band in Kekulé-ordered graphene. (A) A schematic for the flat band near the van Hove singularity point in Kekulé-ordered graphene and constant energy maps of the Dirac cones. (B) The full three-dimensional electronic structure of Kekulé-ordered graphene measured by ARPES. (C) A schematic drawing of Li-intercalated bilayer graphene.

in Fig. 1C. Figure 1B shows an overview of the three-dimensional electronic structure from ARPES measurements. Two large pockets labeled as α and β are observed near each Brillouin zone (BZ) corner indicating large electron doping from the intercalated Li atoms, and the Dirac points are shifted to energies of -1.27 and -1.82 eV (pointed by black and gray arrows in Fig. 1B). The Dirac point energy of -1.82 eV for the β pocket is at even lower energy than the -1.6 eV in the Yb-intercalated case ²¹ suggesting a larger doping, yet here there is no hybridization with the intercalated Li. The absence of hybridization distinguishes it from Ca-intercalated ^{14,15,25} or Yb-intercalated ²¹ graphene, and is in agreement with calculated electronic structure ²⁵. In addition, the β pocket shows a stronger trigonal warping than that obtained in Ca-intercalated bilayer graphene, where the pocket remains quite straight even near the 1/4 doping and charge density wave has been reported ^{14,15}. Moving toward E_F , the β pocket turns into a flat band near the M point (pointed by red arrow in Fig. 1B) and the M* point (equivalent to M point in the superlattice BZ). This is accompanied by folded Dirac cones at Γ , indicating a coexistence of extended flat band and Kekulé order ²². In the following, we focus on the extended flat band and many-body interactions associated with the high density of states near the 1/4 doping, as well as the evolution of the Kekulé order and the flat band upon Li intercalation.

Figure 2A shows the Fermi surface map, which consists of two pockets at each K point and replica pockets at Γ . The carrier concentrations can be directly extracted from the size of the two Fermi pockets through the Luttinger theorem ²⁶. The extracted carrier concentrations are $1.3 \times 10^{14} \text{ cm}^{-2}$ and $4.3 \times 10^{14} \text{ cm}^{-2}$ for α and β pockets respectively, or equivalently 0.07 and 0.23 electrons per unit cell. Even higher carrier concentrations of $1.4 \times 10^{14} \text{ cm}^{-2}$ and $5.1 \times 10^{14} \text{ cm}^{-2}$, or 0.08

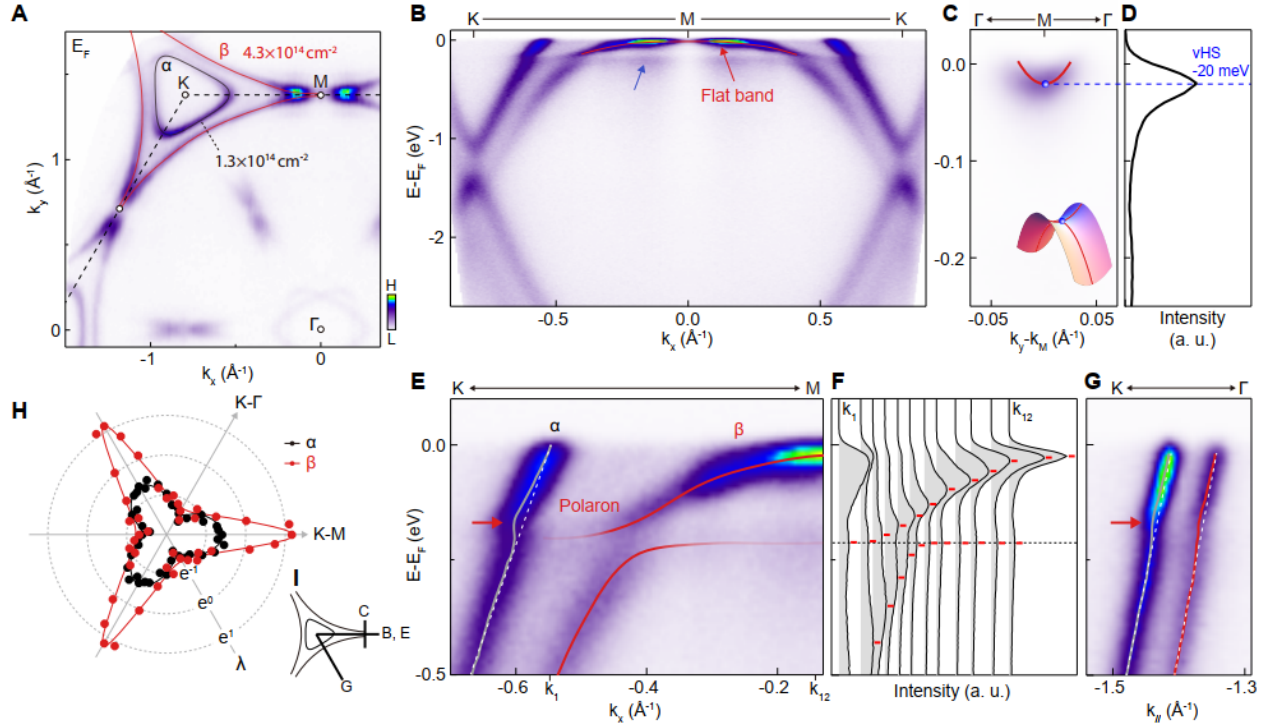


Figure 2: Flat band at VHS and enhanced electron-phonon coupling. (A) Fermi surface map. (B) Dispersion image along the K-M-K direction. (C) Dispersion image along the Γ -M- Γ direction. The inset is a schematic of the saddle point. (D) EDC at the M point, showing that the VHS (blue dot) is at -20 meV. (E) Dispersion image around E_F along the K-M direction. (F) EDCs for data shown in E to visualize the polaron band. (G) Dispersion image around E_F along the K- Γ direction. (H) Extracted angular dependence of el-ph coupling constant of two bands. (I) Schematics for directions of corresponding dispersion images.

and 0.27 electrons per unit cell, can be obtained by second Li intercalation of the same sample after removing the intercalated Li by thermal annealing (see Methods and *SI Appendix*, Fig. S1), which is likely caused by some residual Li ions adsorbed in addition to the newly-intercalated Li. The carrier concentration for the Li-intercalated graphene is in line with the superdense Li intercalate between two graphene sheets in an electrochemical cell with a carrier density of $4 \times 10^{14} \text{ cm}^{-2}$ which is estimated from density functional theory calculation²⁷, while we can resolve each electron pocket and extract the corresponding carrier concentration directly.

The high carrier concentration shifts the VHS at the M point to below E_F . Figure 2B, C shows dispersion images measured along two high symmetry directions through the M point. The dispersion is quite flat when approaching the M point and extended in a large momentum range (extended flat band), and it corresponds to the top of the valence band along the K-M direction (Fig. 2B) and the bottom of the conduction band along the Γ -M direction (Fig. 2C), indicating that it is a saddle point (schematic in the inset of Fig. 2C). Energy distribution curve (EDC) at the M point shows that the saddle point VHS is at -20 meV. This is close to the 1/4 doping which has been extensively investigated theoretically^{8-10,28}. We note that correlated physics and superconductivity have been reported in MABLG^{2,3}, where the flat band is induced by band structure engineering through the Moiré potential. Here we show that by Li intercalation, the flat band at the VHS at the M point can be tuned to near E_F , thus providing an important platform for investigating correlated physics and flat band induced instabilities around the 1/4 doping. The reduction of the π^* band width from $\sim 3 \text{ eV}$ ¹¹ to 1.8 eV (defined by the energy separation between the top of the π^* band -0.02 eV and the Dirac point energy -1.82 eV) suggests that there is a strong reduction

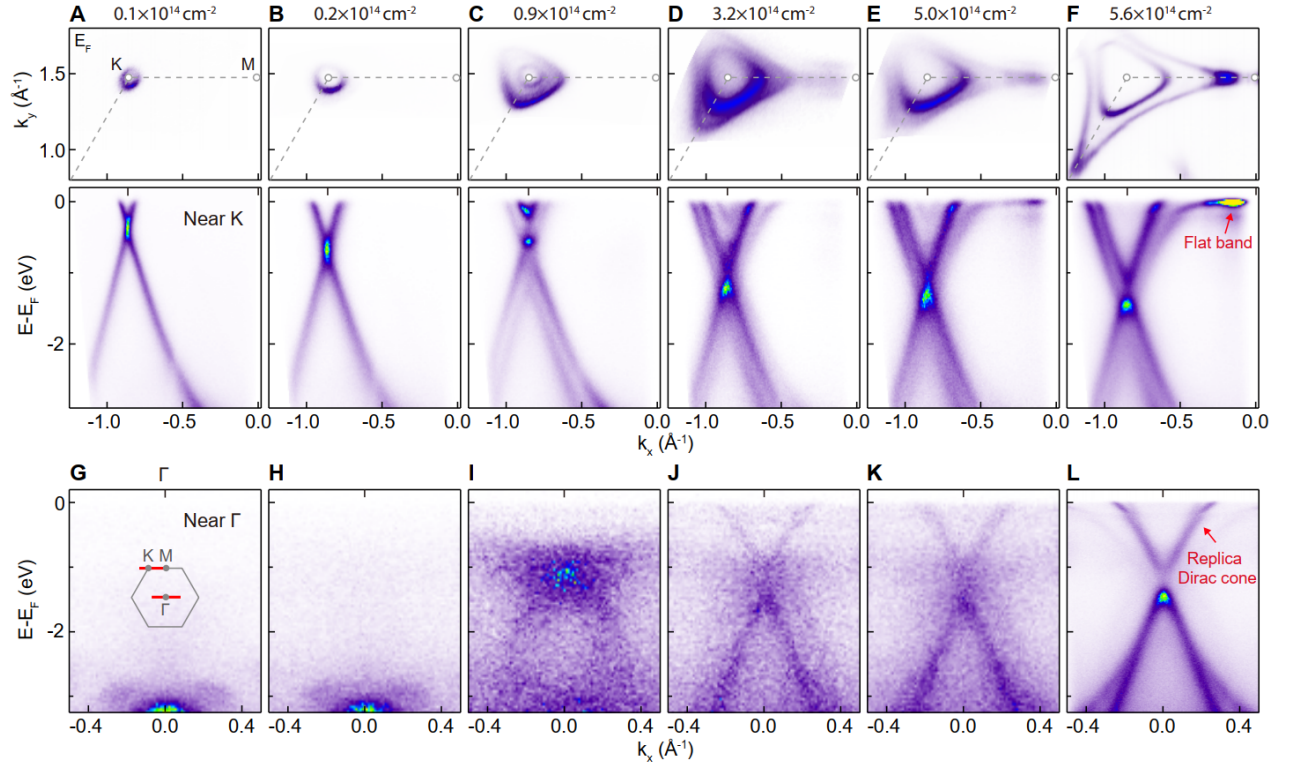


Figure 3: Evolution of flat band and replica Dirac cone during Li deposition process. (A-F) Fermi surface maps around the K point and dispersion images along the K-M direction at different doping levels (total carrier concentration). (G-L) Dispersion images along the Γ -K direction at different doping levels the same as (A-F). The inset in (G) indicates the directions of dispersion images in (A-F) and (G-L).

of the band width due to electron-electron correlation, similar to the case of other doped graphene samples^{12,29,30}. Importantly, the doping for the β pocket is beyond the VHS yet the absence of hybridization or orbital contribution from the intercalated Li compared to the Yb-intercalated graphene²¹ or Ca-intercalated graphene^{14,15,25} allows probing the many-body interactions of the intrinsic Dirac fermions.

The high carrier concentration leads to strong el-ph coupling. Figure 2E shows a zoom-in of the dispersion image near E_F . For the α pocket which does not reach the doping level of the VHS, a renormalization of the dispersion, a kink, is clearly observed (pointed by the red arrow), while for the β band which is beyond the VHS, the el-ph coupling is even stronger, with a strongly deviated dispersion at similar energy. The extracted dispersions for α and β pockets are shown as gray and red curves in Fig. 2E, and a kink is observed at the energy of -180 ± 20 meV. Comparison of this phonon energy with the calculated phonon dispersion for the Kekulé-ordered graphene³¹ shows that the phonons that are coupled with electrons are the in-plane optical phonon A_{1g} . The el-ph coupling strength can be extracted from the renormalization of the Fermi velocity (see *SI Appendix*, Fig. S2 for more details), which gives an el-ph coupling constant of $\lambda_{\alpha}^{KM} = 0.55$ along the K-M direction for the α pocket, and $\lambda_{\beta}^{KM} = 3.19$ for the β pocket. The el-ph coupling strength is reduced to $\lambda_{\alpha}^{K\Gamma} = 0.25$ and $\lambda_{\beta}^{K\Gamma} = 0.27$ along the K- Γ direction (Fig. 2G). The el-ph coupling constant is quite anisotropic, with the anisotropic ratio increasing from 2.2 for the α pocket (black symbols in Fig. 2H) to 11.8 for the β pocket (red symbols in Fig. 2H). The el-ph coupling constant far exceeds previously reported values of $\lambda = 0.14$ to 0.61 for pristine graphene³², alkaline metal doped graphene^{33,34}, superconducting Li or Ca doped graphene^{25,35} and graphite³⁶, which is

associated with the high carrier concentration here. In addition to kinks in the dispersions, band renormalization induced by Holstein polaron, quasiparticles formed by charged carriers dressed by a polarizable medium when the band width is larger than the phonon energy^{37,38}, is observed at energy of -210 ± 20 meV (Fig. 2F) (indicated by blue arrow in Fig. 2B) over a large momentum range. The larger energy of 210 meV indicates the Holstein polaron is formed by E_{2g} phonon at the Γ point^{39,40} which is typically hidden in graphene^{32,34} and suggests that the intra-band scattering caused by the high DOS plays an important role.

In addition to the extended flat band, the Li-intercalated graphene also exhibits Kekulé order. To investigate if there exists a correlation between the extended flat band near the VHS and the Kekulé order, we investigate the evolution of electronic structures measured during the Li intercalation process, as shown in Fig. 3. Here the size of the Fermi pocket is used to quantify the electron doping, while the dispersions near K and Γ are used to monitor the emergence of the extended flat band and the Kekulé order respectively. Before Li intercalation, the monolayer graphene shows electron doping with the Dirac point at -0.38 eV as shown in Fig. 3A. Upon Li deposition, the carrier concentration increases, and at carrier concentration of $n = 0.9 \times 10^{14} \text{ cm}^{-2}$ (see Fig. 3C), a new Dirac cone appears implying decoupling of the buffer layer from the SiC substrate, leading to two graphene layers⁴¹. A broad feature emerges at Γ near -1 eV, which is likely originated from the bonding between Li and SiC substrate⁴¹. Upon further Li deposition, the electron doping increases and the extended flat band starts to appear at a carrier concentration of $n = 3.2 \times 10^{14} \text{ cm}^{-2}$ (Fig. 3D), while at the same time, the replica Dirac cone at the Γ point also becomes observable (Fig. 3J), indicating the formation of the Kekulé order. Further Li deposition leads to larger pock-

ets, and the flat band becomes stronger and finally saturated at $n = 5.6 \times 10^{14} \text{ cm}^{-2}$ (Fig. 3F). The evolution of the flat band at K and folded Dirac cones at Γ suggests a strong correlation between the emergence of the flat band and the Kekulé order.

To further confirm the co-development of the extended flat band and the Kekulé order, Figure 4A shows the continuous evolution of the electronic structure during Li intercalation, and quantitative analysis of the intensity for the extended flat band and the folded Dirac cones is shown in Fig. 4B,C. A comparison of the temporal evolution of the intensity for the extended flat band and replica Dirac cone shows that they have the same trend, and they both increase with the carrier concentration of β pocket (red symbol in Fig. 4B), thereby confirming that the flat band, high carrier density and the Kekulé order all co-develop together.

In summary, we report extended flat band in Kekulé-ordered graphene. The large carrier concentration of $4.3 \times 10^{14} \text{ cm}^{-2}$ shifts the VHS at the M point of graphene to -20 meV, leading to an extended flat band near E_F . Renormalization due to strong many-body interaction is observed in the dispersion. More importantly, the flat band co-develops with the Kekulé order, suggesting a correlation between these two intriguing properties. Our work shows that the Kekulé-ordered graphene is not only an ideal system for probing CSB physics, but also provides a new playground where extended flat band, strong electron-phonon coupling and electron-electron correlation all coexist near the 1/4 doping of graphene, thereby providing opportunities for investigating flat band induced instabilities.

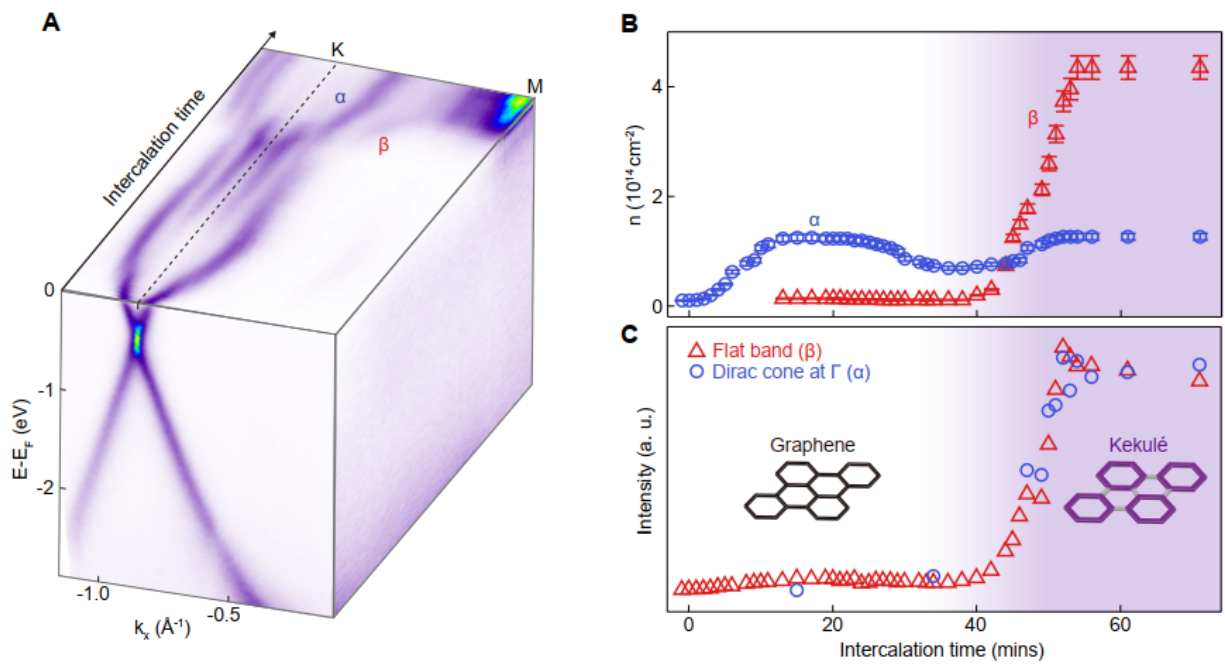


Figure 4: Correlation between flat band and replica Dirac cone. (A) Continuous evolution of the band structures during Li intercalation. (B) Evolution of carrier concentration for two bands α and β during Li intercalation. (C) Intensity evolution of flat band and replica Dirac cone during Li intercalation.

Methods

Sample preparation High-quality graphene was grown by flash annealing the Si face of 6H-SiC(0001) substrates in ultrahigh vacuum. The Kekulé-ordered bilayer graphene is obtained by lithium intercalation of a monolayer graphene sample grown on SiC substrate, which release the bonding between the buffer layer and SiC substrate, resulting in a bilayer graphene sample. The Li intercalation process was performed by *in situ* deposition of Li using an alkali metal dispenser (SAES)^{22,23}, with the graphene samples maintained at 320 K. The intercalation process was monitored by ARPES measurements and low energy electron diffraction (LEED).

ARPES measurements ARPES measurements were performed in the home laboratory at Tsinghua university. The sample was measured at 80 K and in a working vacuum better than 1×10^{-10} Torr with the energy resolution of analyzer set to better than 20 meV. ARPES spectra were measured by unpolarized Helium lamp (21.2 eV).

Acknowledgements We thank Hong Yao and Congjun Wu for useful discussions. This work was supported by the National Natural Science Foundation of China (Grants No. 11725418), the National Key R&D Program of China (Grants No. 2016YFA0301004, 2016YFA0301001, 2020YFA0308800), Tsinghua University Initiative Scientific Research Program, and Tohoku-Tsinghua Collaborative Research Fund. J. L. was supported by the National Natural Science Foundation of China (Grant No. 11874036) and Local Innovative and Research Teams Project of Guangdong Pearl River Talents Program (2017BT01N111).

1. Bistritzer R, MacDonald AH (2011) Moiré bands in twisted double-layer graphene. *Proc. Natl. Acad. Sci. U.S.A.* 108:12233–12237.
2. Cao Y, et al. (2018) Unconventional superconductivity in magic-angle graphene superlattices. *Nature* 556:43.
3. Cao Y, et al. (2018) Correlated insulator behaviour at half-filling in magic-angle graphene superlattices. *Nature* 556(7699):80–84.
4. Jiang Y, et al. (2019) Charge order and broken rotational symmetry in magic-angle twisted bilayer graphene. *Nature* 573(7772):91–95.
5. Black-Schaffer AM, Doniach S (2007) Resonating valence bonds and mean-field d -wave superconductivity in graphite. *Phys. Rev. B* 75(13):134512.
6. Raghu S, Kivelson SA, Scalapino DJ (2010) Superconductivity in the repulsive Hubbard model: An asymptotically exact weak-coupling solution. *Phys. Rev. B* 81(22):224505.
7. Pathank S, Shenoy VB, Baskara G (2010) Possible high-temperature superconductivity with a $d + id$ pairing symmetry in doped graphene. *Phys. Rev. B* 81:085431.
8. Nandkishore R, Levitov LS, Chubukov AV (2012) Chiral superconductivity from repulsive interactions in doped graphene. *Nat. Phys.* 8:158.
9. Wang WS, et al. (2012) Functional renormalization group and variational Monte Carlo studies of the electronic instabilities in graphene near $\frac{1}{4}$ doping. *Phys. Rev. B* 85(3):035414.

10. Jiang S, Mesaros A, Ran Y (2014) Chiral spin-density wave, spin-charge-charge liquid, and $d+id$ superconductivity in $1/4$ -doped correlated electronic systems on the honeycomb lattice. *Phys. Rev. X* 4(3):031040.
11. Castro Neto AH, Guinea F, Peres NMR, Novoselov KS, Geim AK (2009) The electronic properties of graphene. *Rev. Mod. Phys.* 81(1):109–162.
12. McChesney JL, et al. (2010) Extended van Hove singularity and superconducting instability in doped graphene. *Phys. Rev. Lett.* 104(13):136803.
13. Sugawara K, Kanetani K, Sato T, Takahashi T (2011) Fabrication of Li-intercalated bilayer graphene. *AIP Adv.* 1(2):022103.
14. Kanetani K, et al. (2012) Ca intercalated bilayer graphene as a thinnest limit of superconducting C_6Ca . *Proc. Natl. Acad. Sci. U.S.A.* 109(48):19610–19613.
15. Shimizu R, et al. (2015) Charge-density wave in Ca-intercalated bilayer graphene induced by commensurate lattice matching. *Phys. Rev. Lett.* 114(14):146103.
16. Caffrey NM, et al. (2016) Structural and electronic properties of Li-intercalated graphene on SiC(0001). *Phys. Rev. B* 93(19):195421.
17. Hell MG, et al. (2018) Resonance raman spectrum of doped epitaxial graphene at the lifshitz transition. *Nano Lett.* 18(9):6045–6056.
18. Link S, et al. (2019) Introducing strong correlation effects into graphene by gadolinium intercalation. *Phys. Rev. B* 100(12):121407.

19. Hwang C, et al. (2014) Ytterbium-driven strong enhancement of electron-phonon coupling in graphene. *Phys. Rev. B* 90(11):115417.
20. Rosenzweig P, Karakachian H, Link S, Küster K, Starke U (2019) Tuning the doping level of graphene in the vicinity of the van hove singularity via ytterbium intercalation. *Phys. Rev. B* 100(3):035445.
21. Rosenzweig P, Karakachian H, Marchenko D, Küster K, Starke U (2020) Overdoping graphene beyond the van hove singularity. *Phys. Rev. Lett.* 125(17):176403.
22. Bao C, et al. (2021) Experimental evidence of chiral symmetry breaking in Kekulé-ordered graphene. *Phys. Rev. Lett.* 126:206804.
23. Virojanadara C, Watcharinyanon S, Zakharov AA, Johansson LI (2010) Epitaxial graphene on 6H-SiC and Li intercalation. *Phys. Rev. B* 82(20):205402.
24. Fiori S, et al. (2017) Li-intercalated graphene on SiC(0001): An STM study. *Phys. Rev. B* 96:125429.
25. Profeta G, Calandra M, Mauri F (2012) Phonon-mediated superconductivity in graphene by lithium deposition. *Nat. Phys.* 8:131–134.
26. Luttinger JM (1960) Fermi surface and some simple equilibrium properties of a system of interacting Fermions. *Phys. Rev.* 119(4):1153–1163.
27. Kühne M, et al. (2018) Reversible superdense ordering of lithium between two graphene sheets. *Nature* 564(7735):234–239.

28. Gu ZC, et al. (2013) Time-reversal symmetry breaking superconducting ground state in the doped Mott insulator on the honeycomb lattice. *Phys. Rev. B* 88(15):155112.
29. Siegel DA, et al. (2011) Many-body interactions in quasi-freestanding graphene. *Proc. Natl. Acad. Sci. U.S.A.* 108(28):11365–11369.
30. Tang HK, et al. (2018) The role of electron-electron interactions in two-dimensional Dirac fermions. *Science* 361(6402):570–574.
31. Zhang H, et al. (2021) Self-energy dynamics and mode-specific phonon threshold effect in a Kekulé-ordered graphene. *arXiv:2106.01358*.
32. Zhou S, Siegel D, Fedorov A, Lanzara A (2008) Kohn anomaly and interplay of electron-electron and electron-phonon interactions in epitaxial graphene. *Phys. Rev. B* 78(19):193404.
33. Bostwick A, Ohta T, Seyller T, Horn K, Rotenberg E (2007) Quasiparticle dynamics in graphene. *Nat. Phys.* 3(1):36–40.
34. Fedorov AV, et al. (2014) Observation of a universal donor-dependent vibrational mode in graphene. *Nat. Commun.* 5:3257.
35. Ludbrook BM, et al. (2015) Evidence for superconductivity in Li-decorated monolayer graphene. *Proc. Natl. Acad. Sci. U.S.A.* 112(38):11795–11799.
36. Valla T, et al. (2009) Anisotropic electron-phonon coupling and dynamical nesting on the graphene sheets in superconducting CaC₆ using angle-resolved photoemission spectroscopy. *Phys. Rev. Lett.* 102:107007.

37. Wang Z, et al. (2016) Tailoring the nature and strength of electron-phonon interactions in the SrTiO₃(001) 2D electron liquid. *Nat. Mater.* 15:835.
38. Kang M, et al. (2018) Holstein polaron in a valley-degenerate two-dimensional semiconductor. *Nat. Mater.* 17(8):676–680.
39. Maultzsch J, Reich S, Thomsen C, Requardt H, Ordejón P (2004) Phonon dispersion in graphite. *Phys. Rev. Lett.* 92(7):075501.
40. Piscanec S, Lazzeri M, Mauri F, Ferrari A, Robertson J (2004) Kohn anomalies and electron-phonon interactions in graphite. *Phys. Rev. Lett.* 93(18):185503.
41. Bisti F, et al. (2015) Electronic and geometric structure of graphene/SiC(0001) decoupled by lithium intercalation. *Phys. Rev. B* 91:245411.